# ARTICLE

# Creep behavior of a γ′-strengthened Co-base alloy with zero γ/γ′-lattice misfit at 800 °C, 196 MPa

Jan Midtlyng and Alexander I. Epishin[a)]
*Institute of Materials Science and Technologies, Technical University of Berlin, Berlin 10587, Germany*

Nikolay V. Petrushin
*All-Russian Scientific Research Institute of Aviation Materials (VIAM), Department of Superalloys, Moscow 105005, Russia*

Thomas Link
*Institute of Materials Science and Technologies, Technical University of Berlin, Berlin 10587, Germany*

Gert Nolze
*Federal Institute for Materials Research and Testing (BAM), Department of Materials Engineering, Berlin 12205, Germany*

Igor L. Svetlov
*All-Russian Scientific Research Institute of Aviation Materials (VIAM), Department of Superalloys, Moscow 105005, Russia*

Walter Reimers
*Institute of Materials Science and Technologies, Technical University of Berlin, Berlin 10587, Germany*

Deformation and structural behavior of an experimental γ′-strengthened Co-base alloy during creep at 800 °C and 196 MPa have been investigated. The characteristic features of this alloy are zero γ/γ′-lattice misfit and a fine γ/γ′-microstructure. In the initial condition, the γ′-precipitates in this alloy are small (size of about 100 nm), have polyhedral morphology, and are separated by the very narrow γ-channels (width of about 10 nm). The tests performed up to about 1% creep strain (about 500 h creep time) gave creep curves with a slow constant strain rate and without an apparent transient creep, typical for superalloys with nonzero misfit. In this initial stage of creep, entering of the narrow γ-channels by dislocations is blocked by a strong Orowan force. The micromechanism of creep was identified as an octahedral glide of ⟨011⟩ superdislocations simultaneously in two phases, γ and γ′. The γ/γ′-microstructure with zero misfit shows no rafting but rapidly coarsens isotropically. It is concluded that zero misfit is beneficial at the initial stages of the creep but is unfavourable for long-term creep because of the continuous microstructural coarsening.

## I. INTRODUCTION

Recently, Co-base alloys with a γ/γ′-microstructure similar to that of Ni-base superalloys were discovered.[1] In these Co-base alloys, a face-centred cubic (fcc) solid solution of Co, γ, is strengthened by precipitation of a stable ternary $Co_3(Al,W)$ intermetallic compound, γ′, with the ordered structure $L1_2$ ($Cu_3Au$ type). It is assumed that these new γ′-strengthened Co-base alloys can substitute the Ni-base superalloys in some important applications. The reasons for this assumption are:

(i) The discovered Co-base alloys have higher solidus and liquidus temperatures compared with those of Ni-base superalloys, which makes them potentially attractive for high-temperature applications.

(ii) These Co-base alloys have good castability due to the narrow solidification interval and a low degree of segregation during solidification. This is important for manufacturing of the large single-crystal blades needed for power gas turbines.

(iii) These Co-base alloys are γ single phase in a wide temperature interval, and the material is then soft and ductile. This could permit high-temperature processing, e.g., forging or rolling, assuming that these alloys could be developed as wrought or sheet materials.

Research activities on these new Co-based alloys include: alloy development,[1–7] mechanical testing,[2–8] testing of structural stability[9,10] and oxidation,[2,11] and investigations of deformation micromechanisms.[3,12–15] At the current stage of alloy development, several Co-base alloys have been proposed, which have creep strengths at temperatures 800–900 °C approaching those of Ni-base superalloys, e.g., Refs. 3–5.

An interesting feature of new γ′-strengthened Co-base alloys is that the γ/γ′-lattice misfit in these alloys is significantly shifted toward the positive side. For example, in the experimental alloy Co9Al9W0.1B, the "constrained" γ/γ′-misfit (i.e., misfit between the spacings of constrained γ- and γ′-lattices measured in undeformed material) was found to be +0.8%.[12] For comparison, the misfit in the widely used superalloy CMSX-4 is of about −0.25%.[16] Such a big difference between the misfit in the Co- and in Ni-base alloys results from a difference in the partitioning of the elements between the γ- and γ′-phases. As follows from, e.g.,[1–7] elements like Mo, W, Re, although being the matrix elements in Ni-base alloys, in Co-base alloys have a preference to partition into the γ′-phase, by this increasing its lattice spacing more than in the Ni-base. The finding of a positive misfit in Co-base alloys reopens the discussion about the importance of sign and magnitude of γ/γ′ lattice misfit in superalloys, see Mughrabi.[17] Clarification of this question will need theoretical investigations, e.g., similar to Ref. 18, as well as the misfit-relevant experiments. This article presents such an experimental contribution.

The alloy under investigation in this work is a γ′-strengthened Co-base alloy with zero γ/γ′-lattice misfit that was developed recently at the VIAM, Moscow. The points of interest are the deformation behavior, structural behavior, and deformation mechanism of this superalloy at the initial stage of creep at 800 °C under a load of 196 MPa.

## II. EXPERIMENTAL

The alloy under investigation was an experimental Co-base alloy VIAM-M2 (M: Multicomponent) developed at the VIAM in Moscow, with composition as given at the top of Table I. It is seen from Table I that this alloy contains a high concentration of Co, 53.1 at.%, and the sum of the concentrations of Co and another basic element, Ni (15.9 at. %), is 69 at.%, which is typical for Ni-base superalloys. Concentrations of other alloying elements are close to those in Ni-base superalloys. In spite of the compositional and structural (γ/γ′) similarity with Ni-base alloys, the element partitioning in the Co-base alloy essentially differs from that in the Ni-base alloys. It is seen from the results of energy dispersive X-ray (EDX) microanalysis in a transmission electron microscope (TEM), Table I, that typical γ-solid solution strengtheners, W and Mo, have higher concentrations in γ′ than in γ, and Re has significant concentration in γ′ as well, which is different from the element partitioning in Ni-base superalloys, see e.g., Refs. 19 and 20. Results from previous investigations[7,10] of the Co-base alloy VIAM-M1, which has similar composition but without Ti and Cr, are used in this work for comparison of the γ′-morphologies. Its composition is given at the bottom of Table I.

TABLE I. Compositions of Co-base alloys VIAM-M2[this work] and VIAM-M1[11,12] measured by EDX in SEM, and composition of phases γ, γ′ and β in alloy VIAM-M2 measured by EDX in TEM[this work].

| | Al | Ti | Cr | Co | Ni | Mo | Ta | W | Re |
|---|---|---|---|---|---|---|---|---|---|
| **VIAM-M2** | | | | | | | | | |
| Alloy (wt%) | 6.9 | 2.1 | 7.7 | 53.5 | 15.9 | 1.8 | 2.7 | 7.9 | 1.5 |
| Alloy (at.%) | 14.9 | 2.6 | 8.7 | 53.1 | 15.9 | 1.1 | 0.9 | 2.5 | 0.5 |
| γ-phase (at.%) | 9.2 | 0.9 | 14.8 | 58.5 | 12.2 | 1.2 | 0.3 | 2.0 | 0.8 |
| γ′-phase (at.%) | 13.2 | 2.6 | 7.9 | 53.6 | 16.5 | 1.4 | 1.0 | 3.3 | 0.4 |
| $c_{\gamma'}/c_\gamma$ | 1.4 | 2.9 | 0.5 | 0.9 | 1.4 | 1.1 | 4.0 | 1.6 | 0.5 |
| β-phase (at.%) | 42.9 | 3.0 | 2.5 | 33.5 | 16.9 | 0.2 | 0.3 | 0.5 | ≈0 |
| **VIAM-M1** | | | | | | | | | |
| Alloy (wt%) | 6.3 | … | … | 67.5 | 15.9 | 1.0 | 2.3 | 5.9 | 1.0 |
| Alloy (at.%) | 13.6 | … | … | 66.9 | 15.9 | 0.6 | 0.7 | 1.9 | 0.3 |

Single crystals of the experimental Co-alloy were solidified by the Bridgman method with liquid metal cooling. The crystal orientation was set by a seed placed in the crucible bottom, giving [001] oriented crystal growth. The single-crystal ingots were cylinders of diameter 15 mm and length 185 mm. The deviation of the cylinders' axes from [001] did not exceed a few degrees. After casting, the ingots were subjected to homogenization (1300 °C/15 h), followed by aging (700 °C/48 h). After heat treatment, the material consisted of a continuous γ/γ′-microstructure and about 10 area% rest eutectics.

Magnitudes of the "constrained" γ/γ′-lattice misfit,

$$\delta_c = (a_{\gamma'} - a_\gamma)/0.5(a_{\gamma'} + a_\gamma) \quad , \qquad (1)$$

where $a_\gamma$ and $a_{\gamma'}$ are the spacings of the mutually constrained γ- and γ′-lattices, which were measured by X-ray diffraction (XRD) using 222 reflections of Fe $K_\alpha$ and 004 reflections of the Cu $K_\alpha$ radiation. The area irradiated by the X-ray beam was about 8 mm², which covers about 400 dendritic cells, hence the measured misfit value represents the average over the dendritic structure. It was found that $\delta_c \approx +0.27\%$ (average of 0.24 and 0.30%) in the alloy VIAM-M1. In the alloy VIAM-M2, $\delta_c \approx 0\%$ (average of −0.08% and +0.07%).

From the heat-treated ingots of VIAM-M2, cylindrical creep specimens with a gauge diameter of 5 mm and a gauge length of 25 mm were machined. They were tested in a lever arm creep machine under a tensile stress of 196 MPa at 800 °C in air. Two creep tests were performed, interrupted after 500 h and 550 h, respectively, at creep strains of about 1%.

The deformed alloy was investigated by scanning electron microscopy (SEM) and TEM under the aspects of stability of the γ/γ′-microstructure, phase equilibrium, and deformation micromechanisms. The SEM used is a Zeiss LEO GEMINI 1530 VP (Carl Zeiss Meditec, Oberkochen, Germany) equipped with a Bruker x-Flash

5030 detector for EDX microanalysis and an e⁻ Flash HR detector for electron backscatter diffraction (EBSD) with the software Esprit and CrystAlign (Bruker, Berlin, Germany). Specimens for SEM were cut parallel to the longitudinal planes (100), mechanically grinded, and then polished. The final step of preparation was polishing with an emulsion containing 0.25 μm silica powder, necessary to remove the mechanically deformed surface layer, which would distort the EBSD pattern. The TEM used is a Philips CM30 (Philips Electron Optics, Eindhoven, the Netherlands) with an EDX microanalysis system NSS 2.3 from Thermo (Thermo Electron Corporation, Madison, Wisconsin). The TEM foils were cut perpendicular to the specimen axis [001] and then electrolytically thinned in an electropolisher, Struers Tenupol-3 (Struers, Copenhagen, Denmark), with an electrolyte of 10 vol% perchloric acid, 83 vol% ethanol, and 7 vol% glycerine, at −30 °C. Dislocations were observed in a two-beam bright field diffraction contrast, and their Burgers vectors $b$ were determined by the contrast extinction rule $gb = 0$, where $g$ is the reciprocal lattice vector positioned such that it meets the Bragg condition. The glide plane was determined by orienting it in the edge-on position, so the dislocation gliding on it appears straight.

## III. RESULTS

Figure 1 shows creep curves of the alloy VIAM-M2 obtained in two tensile creep tests at 800 °C, 196 MPa, interrupted at a creep strain of about 1%. It exposes that in this strain range, the Co-base alloy deforms with nearly a constant strain rate of about $5.5 \times 10^{-9}$ s$^{-1}$ = $2 \times 10^{-3}$%/h. No transient creep is observed for the first specimen (dashed line); for the second (solid line), one can discern a very small transient creep of about 0.08%.

Figure 2 shows the microstructures of VIAM-M2 and, for comparison, VIAM-M1. VIAM-M2 is depicted in the heat treated state [Fig. 2(a)] and after creep [Figs. 2(b) and 2(c)], VIAM-M2 after heat treatment [Fig. 2(d)] and degradation test (stress-free annealing) [Fig. 2(e)]. The temperature of the degradation test was 800 °C, the same as under the creep test on VIAM-M2.
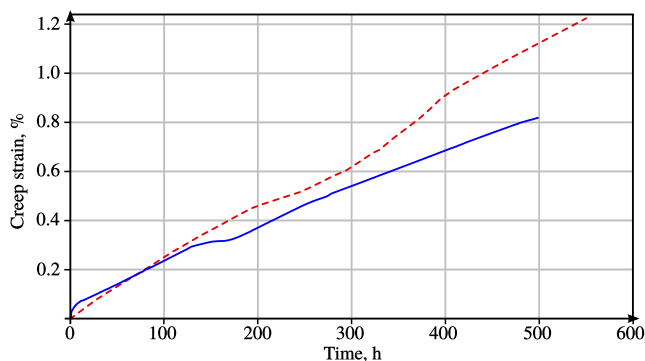


FIG. 1. Creep curves of two [001]-oriented single crystals of the Co-base alloy VIAM-M2 tested at 800 °C/196 MPa.

Comparing the heat treated microstructures of alloys VIAM-M1 with nonzero misfit [Fig. 2(d)] and VIAM-M2 with zero misfit [Fig. 2(a)], it is seen that in the first case, the γ′-precipitates have cuboidal morphology, while in the second case, the γ′-morphology is polyhedral. In both cases, the γ′-precipitates are very fine, and their size is about 100 nm. The γ-channels separating the polyhedral γ′-precipitates in the alloy VIAM-M2 are very narrow, and their width is about 10 nm.

Figure 2(e) shows the γ/γ′-microstructure of the alloy VIAM-M1 after a degradation test (125 h/800 °C), during which it has become rafted even without stress applied. The raft thickness is approximately equal to the initial γ′-size. The stable plate-like γ′-morphology nearly does not change during further annealing at 800 °C up to 1000 h.[10]

The structural behavior of VIAM-M2 is totally different. The initial polyhedral γ′-morphology in this alloy is preserved during creep in spite of significant coarsening, see Fig. 2(b). The γ′-precipitates coarsen almost isotropically, and their size after creep scatters around 0.9 μm (equivalent diameter), which means that the γ′ is coarsened by almost 10 times! It is remarkable that in local areas near the eutectic inclusions, the γ′-morphology is clearly cuboidal [see Fig. 2(c), left], which is typical for superalloys with nonzero misfit, but with increasing the distance from the eutectic, the γ′-precipitates become larger and irregular like in most volume of the material. Obviously, such a microstructural inhomogeneity results from gradients in the chemical composition in the vicinity of the eutectic, which is a consequence of dendritic segregation.

In the alloy VIAM-M2, about 2–3 area% of the needle-shaped phase precipitated in the dendritic arms during creep, see Fig. 3(a). Precipitates of such a morphology were observed in the alloy VIAM-M1 after short tensile tests at 1000 °C,[7] as well as after 1000 h annealing at 800 °C.[10] In Ref. 7, these precipitates were identified in TEM as the β-phase with a crystal structure B2 (CsCl type). In the present work, the needle-shaped precipitates in VIAM-M2 were investigated by EDX in TEM and EBSD in SEM. The TEM investigations confirmed that the observed precipitates are β-phase consisting mostly of Al, Co, and Ni and have a stoichiometry close to Al₃(Co₂Ni), see Table I.

The relative orientations of the γ/γ′-lattice and the β-lattices were investigated by EBSD in SEM. Diffraction patterns were acquired from an area of the specimen, where patterns from several β-precipitates could be obtained in addition to those of the single-crystal γ/γ′-matrix. Figures 3(b)–3(d) display the pole figures for the standard projections $\{100\}_\beta$, $\{111\}_\beta$, and $\{110\}_\beta$, which are preferably used as proof for the corresponding orientation relationship between fcc and body-centred cubic (bcc) crystal structures. The shown pole distributions are very close to the orientation-relationship model proposed by Kurdjumov and Sachs[21]: $\{111\}_{γ/γ′}\|\{110\}_\beta$,
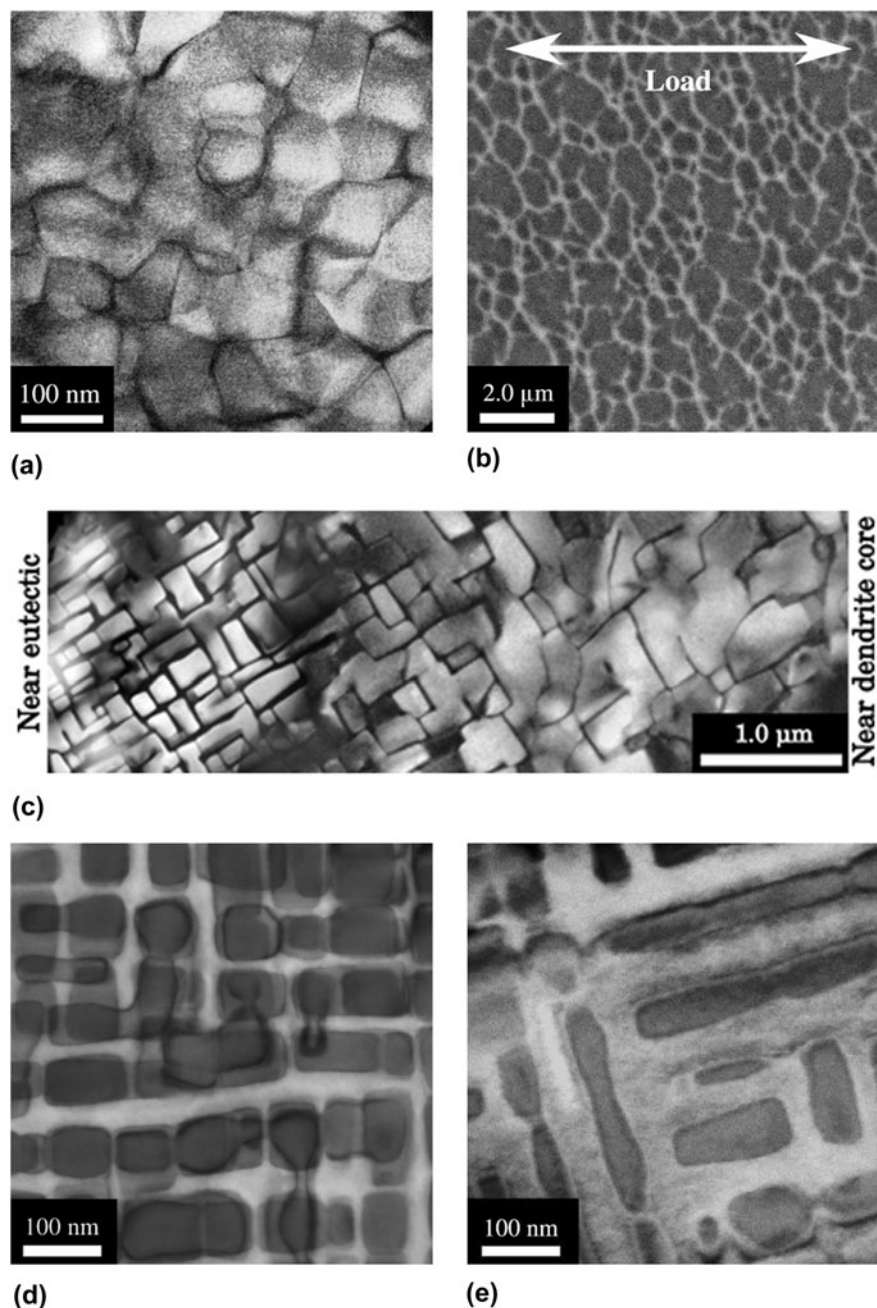
FIG. 2. γ/γ′-microstructure of Co-base alloys before and after testing. (a, b, c) Alloy VIAM-M2. (a) After heat treatment, TEM. (b) After creep test (550 h/800 °C/196 MPa), longitudinal cut (100), and SEM. (c) After creep test, cross section (001), and composed TEM image. (d, e) Alloy VIAM-M1, after heat treatment and after a 125 h degradation test at 800 °C, TEM, quoted from Ref. 10.

$\langle 110 \rangle_{\gamma/\gamma'} \| \langle 111 \rangle_\beta$. It assumes that close-packed lattice planes as well as directions are parallel to each other. The reference axes $x$, $y$, and $z$ are parallel to $\langle 100 \rangle_{\gamma/\gamma'}$. Detailed description of the characterization of the fcc/bcc orientation relationship by EBSD is given in Ref. 22.

Figure 3 gives the orientation relationship between the γ/γ′- and β-lattices but not the growth direction of the needle-shaped β-precipitates. Therefore, identification of the axis direction of the β-needles was performed in the TEM, see Fig. 4. To determine the crystallographic

orientation of the axes of the β-needles, they were oriented in the upright position (parallel to the electron beam) by tilting the TEM foil. This orientation is recognized by the sharp contour of the needle because the precipitate does not overlap with the matrix. In Fig. 4(b), needle I is in an upright position and needles II and III are not. Figure 4(c) shows the corresponding diffraction pattern of needle I. The 6-fold symmetry of the spot positions in the diffraction pattern indicates that the beam is almost parallel to the $\langle 111 \rangle$ zone axis, which
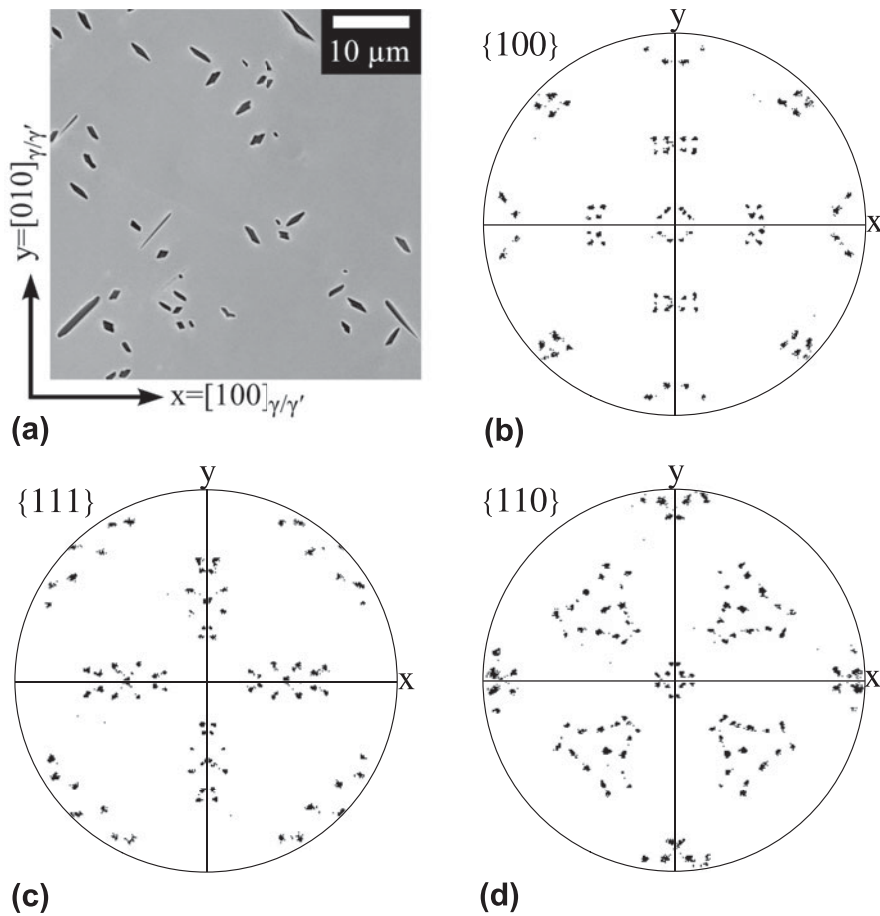
FIG. 3. (a) BSE image of β-needles precipitated in the γ/γ′-microstructure of the Co-base VIAM-M2 alloy after 500 h creep at 800 °C/196 MPa. (b, c, d) $\{100\}_\beta$, $\{111\}_\beta$, and $\{110\}_\beta$ pole figures confirming the Kurdjumov–Sachs orientation relationship $\{111\}_{\gamma/\gamma'}\|\{110\}_\beta$, $\langle 110 \rangle_{\gamma/\gamma'}\|\langle 111 \rangle_\beta$, EBSD.

means that the needle axis coincides with the $\langle 111 \rangle$ axis of the β-lattice. The same result was obtained for several analyzed β-needles. Detailed EBSD analysis showed that the [111] needle axis of a β-precipitate is parallel to one of the six $\langle 110 \rangle$ directions of the γ/γ′-matrix.

Figure 5 shows TEM micrographs of typical dislocation configurations observed in the alloy VIAM-M2 crept for 550 h at 800 °C and 196 MPa. It is seen from Fig. 5 that dislocations propagate simultaneously in two phases, γ and γ′. These images were used for identification of Burgers vectors $\boldsymbol{b}$, line vectors $\boldsymbol{u}$, and glide planes; the results are presented in Table II. Applying the invisibility criterion $\boldsymbol{gb} = 0$, eight dislocations in Fig. 5 were analyzed. In all cases, Burgers vectors $\boldsymbol{b}$ were found to be parallel to crystallographic directions $\langle 011 \rangle$. In Fig. 5(e), the glide plane of dislocations 2 and 3 are in the edge-on position; it is found to be $(\bar{1}1\bar{1})$. The approximate line vector along the length of dislocations 2 and 3 is $[\bar{1}01]$. In Fig. 5(f), a part of dislocation 1 resides in a glide plane which is in the edge-on position; it is found to be $(\bar{1}1\bar{1})$, and the line direction is $[\bar{1}10]$. The glide planes determined by orienting in the edge-on position

are in accordance with the plane normal calculated by $\boldsymbol{b} \times \boldsymbol{u}$. From this, we concluded that dislocations glide on the $\langle 01\bar{1} \rangle\{111\}$ glide system, which is typical for fcc crystals. The dislocations are mostly of mixed type, with 60° deviation between $\boldsymbol{b}$ and $\boldsymbol{u}$. Observation of large areas of TEM foils revealed neither antiphase boundaries (APBs) nor stacking faults, which could indicate γ′ cutting by partial dislocations. Therefore, it was concluded that the dislocations gliding in γ′ are super-disloactions $a\langle 011 \rangle$. A short matrix segment connecting two γ′ dislocations over a narrow γ-channel is assumed to be a couple of $a/2\langle 011 \rangle$ dislocations, where splitting is blocked by a strong Orowan force. Entering of the γ-channels by tongue-shaped dislocation loops was observed very rarely, only in local specific areas with the coarse γ/γ′-microstructure.

## IV. DISCUSSION

It was found that the structural and deformation behavior of the Co-base alloy VIAM-M2 with zero misfit significantly differs from that of Co-base and Ni-base
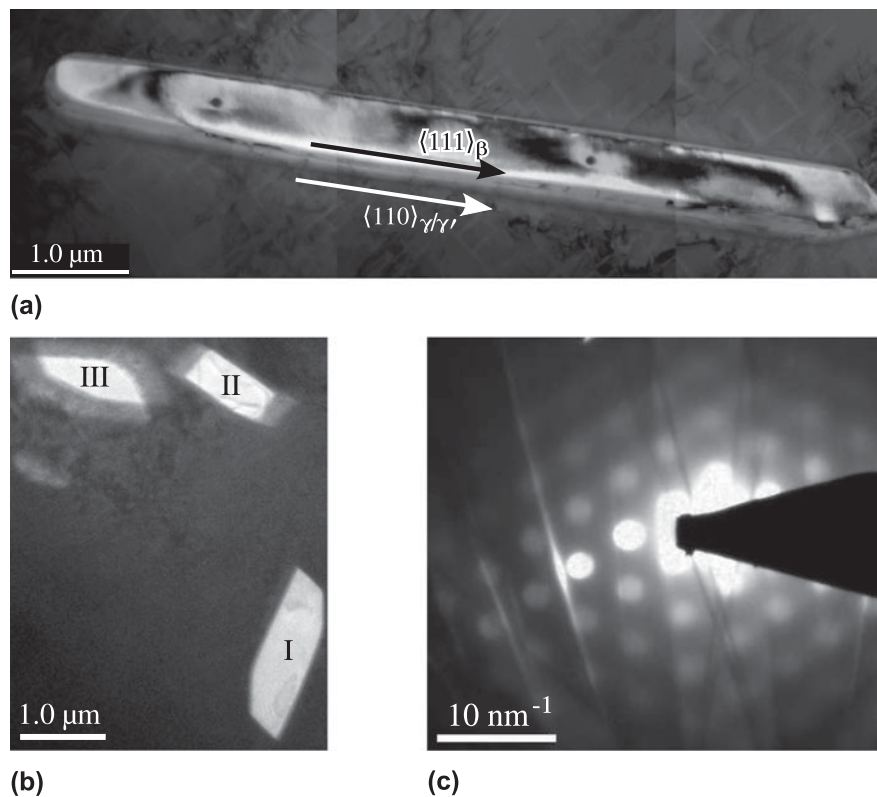
FIG. 4. β-precipitates in the Co-base alloy VIAM-M2 after 550 h creep at 800 °C, 196 MPa (TEM micrographs). (a) Needle lying in the foil's plane (composite image). (b) Needles passing through the foil, I is in an upright position. (c) Diffraction pattern of needle I.

alloys with nonzero misfit. After heat treatment, the γ′-phase has a polyhedral morphology. The polyhedral γ′-particles coarsen isotropically during creep without pronounced rafting. The creep curves are linear (constant strain rate) without essential transient creep. The micro-mechanism of creep is also specific: Dislocation loops do not primarily spread along the matrix channels but just glide simultaneously in both γ and γ′. Although this structural and deformation behavior is quite unusual, it fits well with the parameters of the γ/γ′-microstructure, namely zero misfit and small channel width. This will be shown in the discussion of individual findings in the following four paragraphs.

### A. Polyhedral shape after heat treatment

It is known that the cuboidal γ′-shape with {001} faces is stabilized by misfit stresses. This is because the energy of misfit stresses is minimal when the highly stressed γ-channels have {001} orientation. This, in turn, is because the lattice stiffness is minimal along ⟨001⟩ directions lying in {001} planes. If the γ/γ′-misfit is equal to zero, the γ′-shape is determined by the interface surface tension instead, which should result in a spherical shape. But packing of the equal γ′-spheres is possible only up to 74% volume fraction or even less if the γ-channels between the γ′-precipitates still exist.

The γ′-fraction estimated in the alloy VIAM-M2 from its composition is close to 80 vol%, hence, it exceeds the upper critical value. Therefore during γ′-growth, the approaching surfaces of neighboring γ′-precipitates become flat which leads to a polyhedral shape.

### B. Coarsening without rafting

It is shown in many publications, e.g., in Refs. 23 and 24 that misfit stresses are needed for rafting to take place during creep. When superalloys with a negative misfit are creep deformed under uniaxial stress, a superposition of the applied and misfit stresses acts on the material. When the N-channels (i.e., channels oriented normal to the load axis) undergo plastic deformation, this results in a relaxation of the misfit stresses in the N-channels, which in turn results in the formation of an anisotropic pressure field around the γ′-precipitates. This anisotropic pressure field activates a cross diffusion of alloying elements, resulting in an increase of the width of the relaxed N-channels and narrowing of the stressed P-channels parallel to the load axis. This leads to the change of γ′-shape and finally in coalescence of the neighboring γ′-precipitates, i.e., rafts perpendicular to the load direction. If the γ/γ′-misfit is zero, then no misfit stresses support the applied stress in the N-channels; therefore, no preferable plastification of

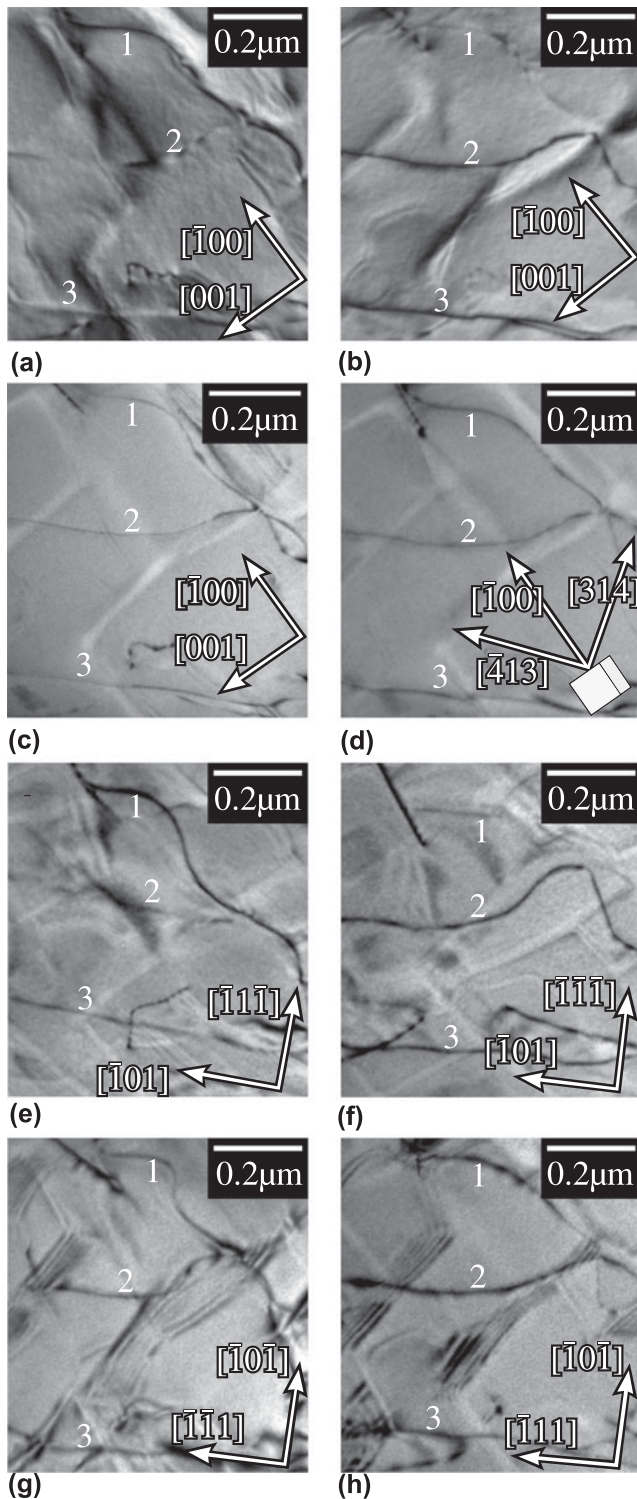**(a)** **(b)** **(c)** **(d)** **(e)** **(f)** **(g)** **(h)**

FIG. 5. Dislocation configurations after 550 h creep at 800 °C, 196 MPa used for identification of Burgers vectors, line vectors, and glide planes (TEM micrographs). Images (a-h) present the same area but under different imaging conditions ($k_0$ and $g$) given in Table II. Note that here, the lattice direction parallel to the stress axis is called [010]. Arrows give the projections of lattice vectors into the image plane. In (d), the orientation of the lattice's unit cell is indicated by a cube.

TABLE II. Identification of Burgers vectors from dislocation contrasts in the TEM. ● stands for visible and ○ for extinct dislocation contrast. Note that here, the lattice direction parallel to the stress axis is called [010]. Line vectors are only approximate.

| | Imaging conditions | | Contrast of dislocation | | |
|---|---|---|---|---|---|
| Image no. | $k_0$ | $g$ | 1 | 2 | 3 |
| 5a | [010] | [002] | ● | ○ | ○ |
| 5b | [010] | [$\overline{2}$00] | ○ | ● | ● |
| 5c | [010] | [$\overline{2}$0$\overline{2}$] | ● | ● | ● |
| 5d | [010] | [202] | ● | ● | ● |
| 5e | [121] | [1$\overline{1}$1] | ● | ○ | ○ |
| 5f | [$\overline{1}$2$\overline{1}$] | [$\overline{1}\overline{1}$1] | ○ | ● | ● |
| 5g | [$\overline{1}$21] | [202] | ● | ● | ● |
| 5h | [12$\overline{1}$] | [$\overline{2}$0$\overline{2}$] | ● | ● | ● |
| $\pm b$ parallel to | | | [01$\overline{1}$] | [110] | [110] |
| Line direction $u$ | | | [$\overline{1}$10] | [$\overline{1}$10] | [$\overline{1}$10] |
| Angle ($b, u$) | | | 60° | 60° | 60° |
| Glide plane | | | (111) | ($\overline{1}$1$\overline{1}$) | ($\overline{1}$1$\overline{1}$) |

the N-channels takes place, and finally no driving force for cross diffusion and rafting evolves.

## C. Cuboidal γ′-shape near the eutectics

It was shown in Refs. 16 and 25 that segregation of alloying elements in Ni-base alloys during dendritic growth results in inhomogeneity of the γ/γ′-misfit within a dendritic cell. The degree of dendritic segregation depends on the alloy composition and somewhat differs for Ni- and Co-base alloys. However, the segregation character is similar for alloys of these two classes, e.g., in Ni-as well as in Co-base alloys, W segregates into the dendritic arms, while Ta segregates into the interdendritic regions, see e.g., Ref. 9. In Ref. 26, quaternary Co–Al–W–Ta alloys were characterized; in particular, the effect of alloy composition on spacing of the γ- and γ′-lattices, $a_\gamma$ and $a_{\gamma'}$, was investigated. Fitting of the results gave the following linear equations:

$$a_{\gamma'}[\text{nm}] = 0.35976 + (-5.1\,c_{\text{Al}} + 2.2\,c_{\text{W}} + 26.4\,c_{\text{Ta}}) \cdot 10^{-5} \quad , \quad (2)$$

$$a_{\gamma}[\text{nm}] = 0.35694 + (3.3\,c_{\text{Al}} + 17.1\,c_{\text{W}} - 2.9\,c_{\text{Ta}}) \cdot 10^{-5} \quad , \quad (3)$$

where $c_i$ is the concentration of the $i$th element in at.%.

It's seen from Eq. (2) that W significantly increases the γ-spacing $a_\gamma$ (preconcentration factor $17.1 \times 10^{-5}$ nm/at.%), while from Eq. (3) it can be followed that Ta significantly increases the γ′-spacing $a_{\gamma'}$ (preconcentration factor $26.4 \times 10^{-5}$ nm/at.%). Taking into account the definition of the γ/γ′-misfit, Eq. (1), one can see that Ta

significantly increases the misfit value $\delta_c$, while W significantly decreases $\delta_c$. Thus, the average misfit in the alloy VIAM-M2 is close to zero, but in the interdendritic region, it can increase due to higher $c_{Ta}$, as well as lower $c_W$. This local increase of the misfit is obviously the reason why the γ/γ′-microstructure is cuboidal and not polyhedral in the interdendritic regions of the VIAM-M2 alloy, that is, close to the eutectic, see Fig. 2(c).

## D. Constant-rate creep curves and dislocation micromechanism of deformation

Under the testing conditions used, the Co-base alloy VIAM-M2 deforms by the glide of dislocation loops on the $\langle 011 \rangle \{111\}$ glide system, as is typical for fcc crystals. It is remarkable that the dislocation loops glide simultaneously in both γ and γ′, keeping a straight shape when they cross the γ-channels. This is different from the dislocation mechanism observed in Ni-base superalloys with nozero misfit, where creep deformation starts by gliding of the dislocation loops in the matrix channels, see, e.g., Refs. 27–29. This primary matrix glide results in a fast transient creep, which then slows down due to a back stress of deposited interfacial dislocations. In VIAM-M2, dislocation loops gliding exclusively in the matrix channels and dislocations deposited in the γ/γ′-interface by the matrix glide were very rarely observed. This suggests that the primary matrix glide was not generally activated in the investigated Co-base alloy, and this explains why transient creep is not observed. There are two obvious reasons for this: First, in an alloy with zero misfit, there is no misfit stress supporting the entering of dislocation loops into the matrix channels. Second, without rafting rapidly widening the matrix channels, the matrix glide can be blocked by a strong Orowan back stress for an extended time, in our case for 500 h. However, at longer creep times, isotropic coarsening will widen the γ-channels, permitting the matrix glide. Such a structural behavior (without rafting) as well as a deformation behavior (without transient creep) was observed in an experimental Ni-base alloy UM-F22 which has γ/γ′-misfit close to zero.[30] During testing at 950 °C and 290 MPa, this alloy showed no rafting and slow creep for 100 h. But after this time, the γ/γ′-microstructure became significantly coarsened, and the creep rate rapidly accelerates. Deformation without the primary matrix glide was reported in Ref. 31 for a high-temperature low-stress creep (1100 °C and 137 MPa) of a superalloy TMS-75 with a small lattice misfit. Due to the small value of γ/γ′-lattice misfit, the dislocations could not glide in the matrix channels but mainly climbed around the γ′-cuboids. In our case, such a climbing is not activated due to a much slower diffusion at 800 °C.

γ′ cutting by $\langle 011 \rangle$ superdislocations is a classical mechanism first reported by Kear and Wilsdorf for the L1$_2$ structure of Cu$_3$Au[32] and then reported for Ni-base superalloys many times, see e.g., Ref. 33. However, this mechanism identified in our work differs from that reported recently for the creep of Co-base alloys at 900 °C.[13–15] The authors found γ′ cutting by $a/2\langle 011 \rangle$ and $a/2\langle 112 \rangle$ dislocations, accompanied by the formation of APBs and stacking faults. Here, one should notice that a stress level applied in our case, 196 MPa, is significantly lower than stress levels applied in Refs. 13–15, between 275 and 345 MPa. It is well known that high stresses are needed to press the partial dislocations inside a superlattice. Moreover, at 800 °C, the temperature of our creep tests, the Co-base alloys show the maximum yield stress,[3] which indicates a high shear strength of the γ′-phase.

## V. CONCLUSIONS

(1) An experimental Co-base alloy with zero γ/γ′-lattice misfit showed unusual structural and deformation behavior, namely: After heat treatment, the γ′-phase in this alloy has a polyhedral morphology. During creep at 800 °C and 196 MPa, the polyhedral γ′-precipitates coarsen isotropically without pronounced rafting. Tests at 800 °C and 196 MPa performed up to about 1% creep strain give creep curves with a constant strain rate and without transient creep. Creep micromechanism is a glide of dislocations simultaneously in the two phases, γ and γ′, without preliminary spreading of dislocation loops along the matrix channels. All these features can be well explained by the zero γ/γ′-lattice misfit and fine γ/γ′-microstructure.

(2) It is reasonable to ask: does an alloy with zero misfit have advantages compared with an alloy with nonzero misfit? One obvious advantage is the absence of a fast transient creep which is caused by two factors: (i) Zero misfit stresses and (ii) thinner channels during isotropic coarsening (without rafting). However, these factors grant a positive contribution only at the initial stage of the creep.

In superalloys with nonzero misfit, the misfit stresses initially promote dislocation glide, but relax during primary creep. Subsequently, even back stresses are induced, which retard dislocation glide in the matrix. Rafting in these alloys rapidly widens the matrix channels, but then, the channel widening slows down because the rafts are stable. In zero misfit alloys, however, the polyhedral γ′-precipitates coarsen continuously. Therefore, one should expect that after a certain time, the channel width in their polyhedral microstructure can be larger than in rafted microstructures, hence their relative advantage would be lost.

(3) During high-temperature exposure, the phase transformation γ′ → β occurs in Co-base alloys. It was found that the β-needles grow in the $\langle 111 \rangle$ directions of the B2

lattice, which correspond to the ⟨110⟩ directions of the γ/γ′-matrix. The β-precipitation after 550 h creep at 800 °C/196 MPa was not found to be strong, 2–3 area % in the dendrite arms.

## ACKNOWLEDGMENTS

## REFERENCES

1. J. Sato, T. Omori, K. Oikawa, I. Ohnuma, R. Kainuma, and K. Ishida: Cobalt-base high-temperature alloys. *Science* **312**(5770), 90 (2006).
2. T.M. Pollock, J. Dibbern, M. Tsunekane, J. Zhu, and A. Suzuki: New Co-based high-temperature alloys. *JOM* **62**(1), 58 (2010).
3. A. Suzuki and T.M. Pollock: High-temperature strength and deformation of γ/γ′ two-phase Co–Al–W-base alloys. *Acta Mater.* **56**(6), 1288 (2008).
4. A. Bauer, S. Neumeier, F. Pyczak, R.F. Singer, and M. Göken: Creep properties of different γ′-strengthened Co-base superalloys. *Mater. Sci. Eng., A* **550**, 333 (2012).
5. A. Bauer, S. Neumeier, F. Pyczak, and M. Göken: Microstructure and creep strength of different γ/γ′-strengthened Co-base superalloy variants. *Scr. Mater.* **63**(12), 1197 (2010).
6. K. Shinagawa, T. Omori, K. Oikawa, R. Kainuma, and K. Ishida: Ductility enhancement by boron addition in Co–Al–W high-temperature alloys. *Scr. Mater.* **61**(6), 612 (2009).
7. N. Petrushin, K. Hvatzkiy, V. Gerasimov, T. Link, A. Epishin, G. Nolze, and G. Gerstein: A single-crystal Co-base superalloy strengthened by γ′ precipitates: Structure and mechanical properties. *Adv. Eng. Mater.* **17**(6), 755 (2015).
8. M.S. Titus, A. Suzuki, and T.M. Pollock: Creep and directional coarsening in single crystals of new γ–γ′ cobalt-base alloys. *Scr. Mater.* **66**(8), 503 (2012).
9. I. Lopez-Galilea, C. Zenk, S. Neumeier, S. Huth, W. Theisen, and M. Göken: The thermal stability of intermetallic compounds in an as-cast SX Co-base superalloy. *Adv. Eng. Mater.* **17**(6), 741 (2015).
10. A.I. Epishin, N.V. Petrushin, T. Link, G. Nolze, Y.V. Loshchinin, and G. Gerstein: Thermal stability of the structure of a heat-resistant cobalt alloy hardened with intermetallic γ′-precipitates. *Russ. Metall.* **2016**(4), 286 (2016).
11. L. Klein, A. Bauer, S. Neumeier, M. Görken, and S. Virtanen: High temperature oxidation of γ/γ′-strengthened Co-base superalloys. *Corros. Sci.* **53**, 2027 (2011).
12. F. Pyczak, A. Bauer, M. Göken, S. Neumeier, U. Lorenz, M. Oehring, N. Schell, A. Schreyer, A. Stark, and F. Symanzik: Plastic deformation mechanisms in a crept L1₂ hardened Co-base superalloy. *Mater. Sci. Eng., A* **571**, 13 (2013).
13. Y.M. Eggeler, M.S. Titus, A. Suzuki, and T.M. Pollock: Creep deformation-induced antiphase boundaries in L1₂-containing single-crystal cobalt-base superalloys. *Acta Mater.* **77**, 352 (2014).
14. M.S. Titus, Y.M. Eggeler, A. Suzuki, and T.M. Pollock: Creep-induced planar defects in L1₂-containing Co- and CoNi-base single-crystal superalloys. *Acta Mater.* **82**, 530 (2015).
15. Y.M. Eggeler, J. Müller, M.S. Titus, A. Suzuki, T.M. Pollock, and E. Spiecker: Planar defect formation in the γ′ phase during high temperature creep in single crystal CoNi-base superalloys. *Acta Mater.* **113**, 335 (2016).
16. U. Brückner, A. Epishin, and T. Link: Local X-ray diffraction analysis of the structure of dendrites in single-crystal nickel-base superalloys. *Acta Mater.* **45**(2), 5223 (1997).
17. H. Mughrabi: The importance of sign and magnitude of γ/γ′ lattice misfit in superalloys with special reference to the new γ′-hardened cobalt-base superalloys. *Acta Mater.* **81**, 21 (2014).
18. S. Gao, M. Fivel, A. Ma, and A. Hartmaier: Influence of misfit stresses on dislocation glide in single crystal superalloys: A three-dimensional discrete dislocation dynamics study. *J. Mech. Phys. Solids* **76**, 276 (2015).
19. U. Hemmersmeier and M. Feller-Kniepmeier: Element distribution in the macro- and microstructure of nickel base superalloy CMSX-4. *Mater. Sci. Eng., A* **248**, 87 (1998).
20. C. Schulze and M. Feller-Kniepmeier: Transmission electron microscopy of phase composition and lattice misfit in the Re-containing nickel-base superalloy CMSX-10. *Mater. Sci. Eng., A* **281**, 204 (2000).
21. G. Kurdjumov and G. Sachs: Über den Mechanismus der Stahlhärtung. *Z. Phys.* **64**(5), 325 (1930).
22. G. Nolze: Characterization of the fcc/bcc orientation relationship by EBSD using pole figures and variants. *Z. Metallkd.* **95**, 744 (2004).
23. S. Socrate and D.M. Parks: Numerical determination of the elastic driving force for directional coarsening in Ni-superalloys. *Acta Metall. Mater.* **41**(7), 2185 (1993).
24. F.R.N. Nabarro: Rafting in superalloys. *Metall. Mater. Trans. A* **27**(3), 513 (1996).
25. U. Brückner, A. Epishin, T. Link, and K. Dressel: The influence of the dendritic structure on the γ/γ′-lattice misfit in the single-crystal nickel-base superalloy CMSX-4. *Mater. Sci. Eng., A* **247**(1–2), 23 (1998).
26. Report on DFG Project: Characterisation of the quaternary system Co–Al–W–Ta for development of γ′-strengthened Co-base alloys, EP 136/2–1, NO 307/5-1, TU Berlin, BAM Berlin, VIAM Moscow (2016).
27. T. Link, A. Epishin, and B. Fedelich: Inhomogeneity of misfit stresses in nickel-base superalloys: Effect on propagation of matrix dislocation loops. *Philos. Mag.* **89**(13), 1141 (2009).
28. M. Feller-Kniepmeier and T. Link: Dislocation structures in γ–γ′ interfaces of the single-crystal superalloy SRR 99 after annealing and high temperature creep. *Mater. Sci. Eng., A* **113**, 191 (1989).
29. M. Probst-Hein, A. Dlouhy, and G. Eggeler: Interface dislocations in superalloy single crystals. *Acta Mater.* **47**(8), 2497 (1999).
30. L.J. Carrol, Q. Feng, and T.M. Pollock: Interfacial dislocation networks and creep in directionally coarsened Ru-containing nickel-base single-crystal superalloys. *Metall. Mater. Trans. A* **39**, 1290 (2008).
31. J.X. Zhang, H. Harada, Y. Koizumi, and T. Kobayashi: Dislocation motion in the early stages of high-temperature low-stress creep in a single-crystal superalloy with a small lattice misfit. *J. Mater. Sci.* **45**(2), 523 (2010).
32. B.H. Kear and H.G.F. Wilsdorf: Dislocation configurations in plastically deformed polycrystalline Cu₃Au alloys. *Trans. AIME* **224**, 382 (1962).
33. G. Scheumann-Frerker, H. Gabrisch, and M. Feller-Kniepmeier: Dislocation microstructures in a single-crystal nickel-base superalloy after tensile testing at 823 K in the [001] direction. *Philos. Mag.* **65**(6), 1353 (1992).